ELSEVIER

Journal of Alloys and Compounds 303–304 (2000) 340–344

Journal of ALLOYS AND COMPOUNDS

www.elsevier.com/locate/jallcom

A Raman spectroscopic study of rare earth mixed oxides

Jan-Christoph Panitz*, Jean-Claude Mayor, Beda Grob, Wilhelm Durisch

Sektion Elektrochemie, Paul Scherrer Institut, CH-5232 Villigen PSI, Switzerland

Abstract

Raman and emission spectroscopy was used for the characterization of dysprosium–yttrium, holmium–yttrium, and ytterbium–yttrium mixed oxides. The samples, which are potential emitter materials for thermophotovoltaic generators, were prepared by combustion synthesis. Due to the similar ionic radii of the trivalent rare earth cations employed, substitutional solid solutions are formed. With changing yttrium content, continuous changes in Raman band position and linewidth occur for the mixed oxides, which were analyzed for selected vibrational modes. By this method, it is possible to determine the composition of the samples. In addition, emission spectroscopy was used for the characterization of the holmium–yttrium mixed oxides. A correlation between the holmium concentration in the yttrium oxide matrix and spectral features was established. By using confocal emission microscopy, local variations in emission band profiles, which may be related to variations in chemical composition, were investigated with micrometer resolution.

Keywords: Solid solutions; Combustion synthesis; Scanning electron microscopy; Candoluminescence; Raman spectroscopy; Emission microscopy

1. Introduction

Several oxides of the f-elements are candoluminescent materials. When heated in a flame or by other energy sources, emission is observed in narrow bands at energies corresponding to f–f transitions characteristic for the given rare earth element [1]. The Welsbach mantle is the most well known application of this property. Another application of such materials is the use as the emitter in a thermophotovoltaic (TPV) energy converter. A TPV generator is based on the principle of converting a selected part of the thermal radiation of an emitter with suitable photovoltaic cells into electricity [2]. The need for small portable power generators has stimulated new interest in TPV energy conversion [3]. The objective of the TPV project carried out at the Paul Scherrer Institut is to demonstrate the feasibility of a residential heating system equipped with an add-on thermophotovoltaic module [4]. Emitter materials based on ytterbium oxide are used in conjunction with silicon solar cells. Part of this project deals with the development and characterization of efficient emitter materials [5]. In this context, an investigation of combustion-synthesized ytterbium–yttrium mixed oxides was performed, using Raman spectroscopy as the principal tool [6].

The purpose of this paper is to describe the extension of the characterization method used to the mixed oxides of dysprosium and yttrium, and holmium and yttrium. The similar ionic radii again result in the formation of substitutional solid solutions, which crystallize in the same space group (T_h^7). The question addressed here is if the features observed with Raman spectroscopy follow a general pattern in RE mixed oxide phases, or whether each sample series shows a different behavior. In addition, very little is known about the mechanisms taking place during combustion synthesis, which is an autothermal process. Up to now, the homogeneity of materials prepared by such processes has been regarded as high, but has not been investigated using spatially resolved spectroscopical techniques. In the case of samples prepared from holmium and yttrium precursors, we have correlated band ratios of Ho^{3+} emission lines recorded in the range 525–555 nm ($^5I_8-^5F_4$ and $^5I_8-^5S_2$ transitions) with chemical composition. Confocal emission microscopy was therefore used to obtain information on the homogeneity of the samples prepared, with a lateral resolution of 1 μm.

2. Experimental

Precursor solutions were prepared by dissolving the necessary amounts of the metal nitrates (dysprosium nitrate hydrate, holmium nitrate hydrate, ytterbium nitrate hydrate

*Corresponding author.

0925-8388/00/$ – see front matter
PII: S0925-8388(00)00606-X

and yttrium nitrate hydrate, all obtained from Aldrich, purity 99.9%) and glycine (Fluka, analytical grade) in water. The mixture was placed in a large stainless steel beaker and heated until ignition occurred, as described by Chick et al. [7], following the safety precautions set out therein. In order to reduce the residual carbon content, the materials were calcined at 1173 K for 5 h. The morphology of the materials was examined by scanning electron microscopy (SEM). Selected samples of holmium–yttrium mixed oxides were pressed into disks and annealed at 1570±30 K for 24 h. For comparison, reference materials (Y_2O_3 and Dy_2O_3 obtained from STREM, Ho_2O_3 and Yb_2O_3 from Aldrich) were obtained with at least 99.99% purity.

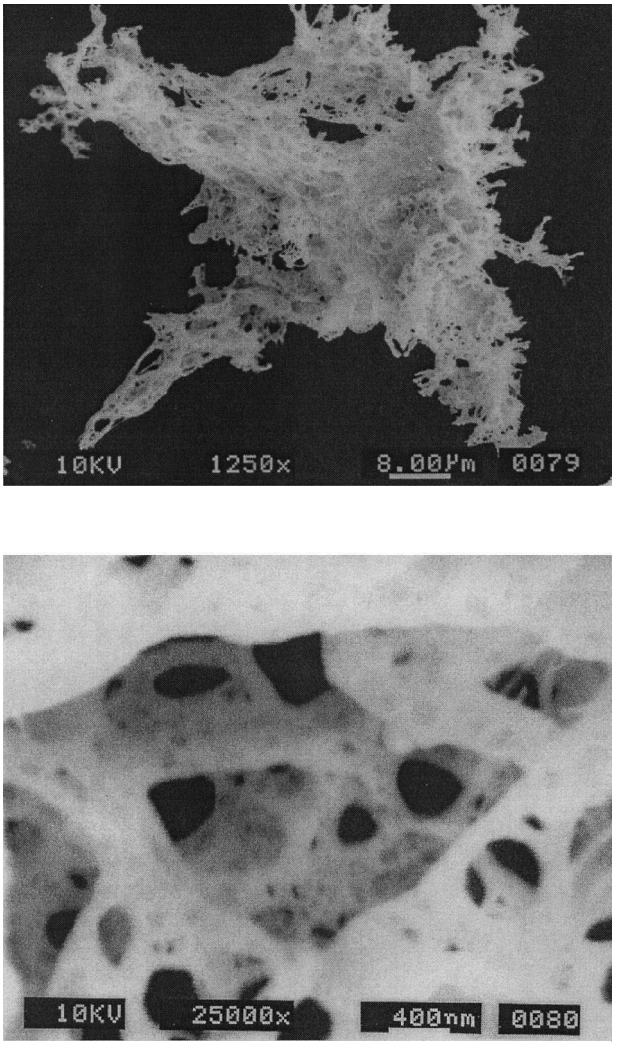

Fig. 1. SEM images obtained from a particle of a combustion-synthesized Ho_2O_3 sample. On the upper micrograph, a particle with approximate dimensions 40×40 μm is shown. The numerous protrusions are typical for materials obtained with this preparation method. In the lower micrograph, the spongy and foam-like microstructure of this particle is revealed.

The Raman and emission spectra were recorded with a Raman confocal microscope (Labram II, Dilor/Instruments S.A.) using a Kr^+ ion laser. The setup has already been described in detail [8]. The Raman spectra of samples containing ytterbium and dysprosium were recorded using the 647.1 nm line, whereas Raman spectra of holmium–yttrium mixed oxides were measured with the 568.2 nm line. For all these experiments, a microscope lens with 50× magnification was used. The 413.1 nm laser emission was used for excitation of the holmium emission spectrum. In the emission mapping experiment, a 100× microscope objective was used to achieve a spatial resolution of 1 μm in the plane of the sample. Maps of 20×15 points were sampled on an area of 20×15 μm. Calibration was performed by recording the line spectra of a neon lamp (PenRay, ORIEL). Raman band positions and linewidths were determined using the Peak Fitting Module of the Origin™ program package (version 5.0, Microcal Inc.). Voigt profiles with fixed Gaussian linewidths corresponding to the spectral resolution were employed in these calculations.

3. Results and discussion

In Fig. 1, the morphology of the particles is illustrated for Ho_2O_3 synthesized by combustion synthesis. The particle shown in the upper micrograph is typical for all samples prepared by combustion synthesis, where rather large (typical dimensions 5–50 μm) and highly porous particles with many protrusions are obtained. In the lower SEM image, the microstructure of the particle is shown. The material is of a spongy nature with struts about 0.2–2 μm wide.

Raman spectra of the reference materials Dy_2O_3,

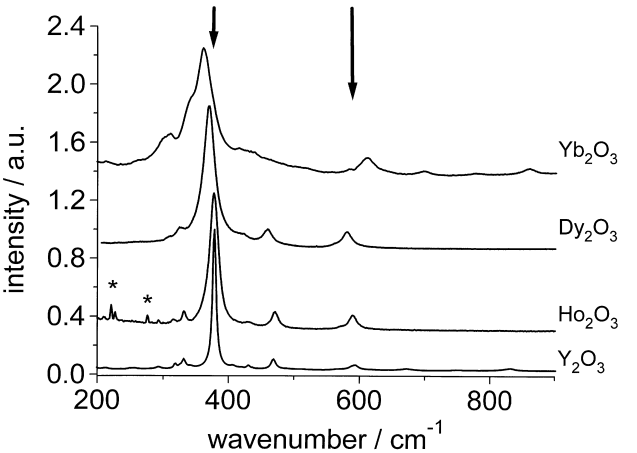

Fig. 2. Raman spectra of reference materials Yb_2O_3, Dy_2O_3, Ho_2O_3 and Y_2O_3. Traces are normalized with respect to the height of the most intense band. The arrows denote the bands analyzed. The features denoted by an asterisk in the Raman spectrum of Ho_2O_3 are artefacts.

Ho_2O_3, Yb_2O_3, and Y_2O_3 in the wavenumber range 200–900 cm^{-1} are given in Fig. 2. The spectra shown are normalized with respect to the height of the most intense band, and the arrows indicate vibrational bands where changes occur. It is interesting to note that the linewidth of the most intense band increases in the sequence Y–Ho–Dy–Yb, whereas its band position decreases. The reference spectra shown agree with those reported in the literature [9–14]. For selected samples prepared by combustion synthesis, calculated band positions and linewidths of the band at about 375 cm^{-1} are reproduced in Table 1. Only results obtained for the most intense band are discussed in the following, since this mode is more sensitive to composition than the mode observed around 600 cm^{-1}; also, the error in the calculation of the linewidth is significantly smaller. In order to compare the behavior of the mixed oxide systems investigated up to now, data from Table 1 are reproduced in Fig. 3, along with values obtained in the phase diagram Yb_2O_3–Y_2O_3 taken from previous work [6]. With increasing lanthanide concentration in the Y_2O_3 host, the band position decreases continuously for all mixed oxide phases, but only for the system Dy_2O_3–Y_2O_3 is an approximately linear relation between band position and composition observed. In the cases of holmium and ytterbium, the present data suggest a quadratic relation between band position and composition, with effects being most pronounced in the case of Yb_2O_3–Y_2O_3. Tentatively, we propose that these differences are due to the fact that the ionic radius of Dy^{3+} is larger, whereas the ionic radii of Ho^{3+} and Yb^{3+} are smaller, than the ionic radius of Y^{3+}.

The linewidths follow a similar pattern for all three phase diagrams investigated: the data presented show an inflection at about 50 mol% substitution (Fig. 3, upper diagram). This inflection is weakest for the system Dy_2O_3–Y_2O_3, and most pronounced for the system Yb_2O_3–Y_2O_3. Continuous changes of band position with composition are typical for substitutional solid solutions, and often the linewidth observed for such systems exhibits a local maximum at 50 mol% substitution [15]. That the effects observed are most pronounced for the Yb_2O_3–Y_2O_3 phase cannot be attributed solely to a mass effect. The contraction of the unit cell plays a role, as first noted by Gouteron et al. [10]. In addition, chemical bonding in the Yb_2O_3–Y_2O_3 phase changes with increasing ytterbium content. Ytterbium has a more deformable electron shell than yttrium [13,16] and, therefore, chemical bonding in Yb_2O_3 is regarded as more covalent than in Y_2O_3. In the dysprosium- and holmium-containing mixed oxides, chemical bonding is more ionic in character, but unit cell dimensions of the end members differ only by +0.6 and +0.04%, respectively. Because the total change in wavenumber across the phase diagram amounts to 5.3 cm^{-1} for Dy_2O_3–Y_2O_3, and to 2.5 cm^{-1} for Ho_2O_3–Y_2O_3, we conclude that the observed wavenumber shift contains information on a subtle change in chemical bonding. It is remarkable that even such small changes in composition can be traced with Raman spectroscopy and subsequent data analysis. For samples with the same thermal history, this method is a useful analytical technique.

Table 1
Band position and linewidths (both in cm^{-1}) of the vibrational mode observed at about 375 cm^{-1} in Dy_2O_3–Y_2O_3 and Ho_2O_3–Y_2O_3 solid solutions

mol% RE	Dy_2O_3–Y_2O_3		Ho_2O_3–Y_2O_3	
	Band position	Linewidth	Band position	Linewidth
0	377.99±0.01	4.77±0.06	377.19±0.02	4.12±0.17
2	377.85±0.02	5.49±0.09	377.17±0.02	4.79±0.13
5	378.03±0.01	5.48±0.03	377.11±0.05	4.14±0.40
10	377.58±0.02	6.39±0.08	377.14±0.02	5.22±0.12
20	377.02±0.01	8.12±0.03	376.97±0.03	6.61±0.18
50	375.32±0.02	13.16±0.1	376.45±0.03	12.54±0.13
100	372.71±0.04	19.85±0.2	374.64±0.04	16.07±0.15

Emission spectra of Ho_2O_3–Y_2O_3 samples excited with the 413.1 nm line are shown in Fig. 4, with three traces

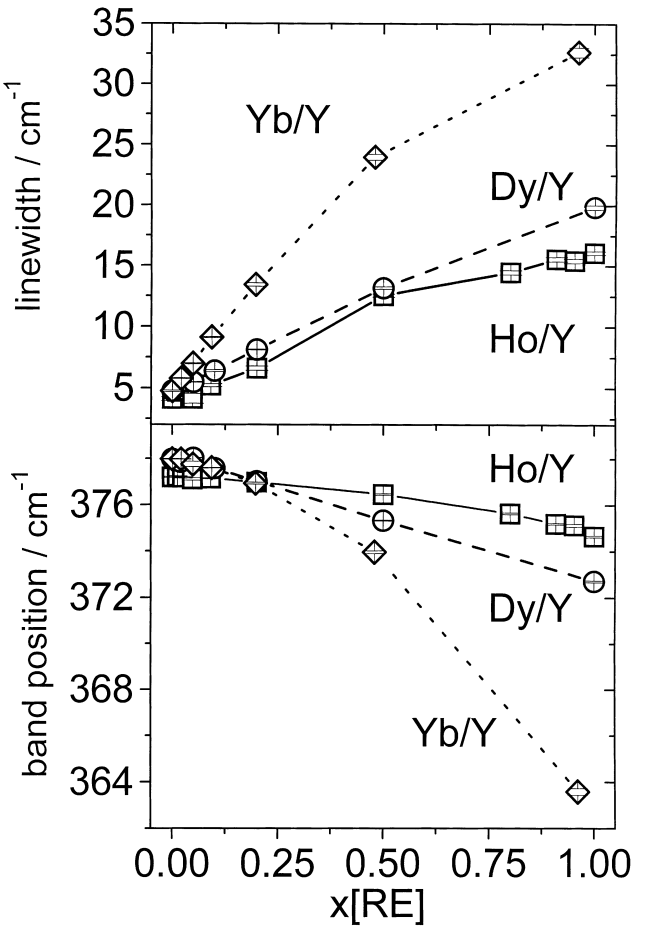

Fig. 3. Band position and linewidth obtained for the most intense Raman band plotted against the RE mole fraction. Squares connected by solid line, holmium–yttrium mixed oxides; circles (dash line), dysprosium–yttrium mixed oxides; diamonds (dotted line), ytterbium–yttrium mixed oxides [6].

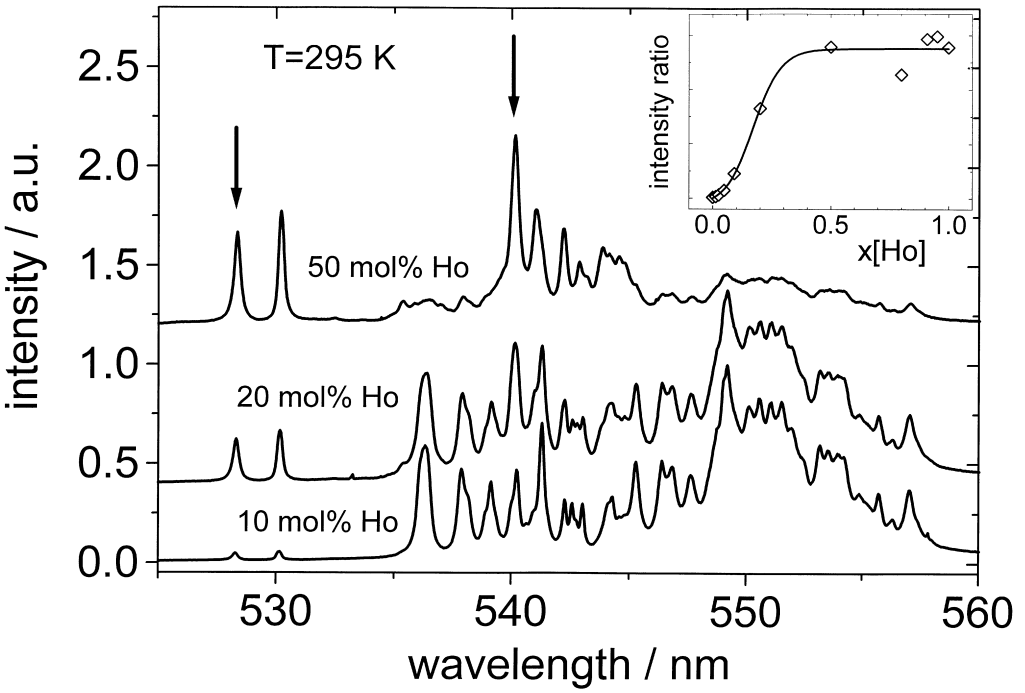

Fig. 4. Emission spectra recorded at room temperature for several Ho–Y mixed oxide samples. The arrows denote the bands used for the calculation of the intensity ratio $I(528)/I(540)$ (cf. text), which is plotted in the inset against Ho mole fraction. Diamonds represent experimental data for samples calcined at 1173 K, and the line is an empirical fit to the data using a sigmoidal function.

selected for display. The emission bands from the $^5F_4$ and $^5S_2$ multiplets fall into the wavelength range observed. The holmium concentration increases from bottom to top, with values of 10, 20 and 50 mol%. Two bands at 528.3 and 530.2 nm are first observed at a concentration of about 1 mol% Ho. Their intensity increases with increasing Ho concentration, up to a concentration of 50 mol% Ho. In addition, changes in the band profile of the $^5I_8$–$^5F_4$ and $^5I_8$–$^5S_2$ transitions are evident. With increasing Ho concentration, the maximum of the band profile shifts from 549.1 to 540.2 nm. An intensity ratio was calculated using the intensity of the band at 528.3 nm [$I(528)$], divided by the intensity of the band at 540.2 nm [$I(540)$]. This intensity ratio is plotted against holmium content in the inset of Fig. 4. Diamonds represent the experimentally obtained data, whereas the solid line is an empirical fit to the data, using a sigmoidal function with equation

$$I(528)/I(540) = (A_1 - A_2)/(1 + \exp((x[\mathrm{Ho}] - x_0)/w)) + A_2$$

Parameters obtained are $A_1 = -0.010 \pm 0.027$, $A_2 = 0.384 \pm 0.010$, $x_0 = 0.157 \pm 0.016$, $w = 0.045 \pm 0.012$, with $\chi^2 = 5.97 \times 10^{-4}$. It is thought that the intensity ratio $I(528)/I(540)$ mirrors the energy transfer between Ho^{3+} centers. Beyond a percolation threshold, $I(528)/I(540)$ is constant.

This relation can be applied to investigate the variations in chemical composition of combustion-synthesized powders with confocal emission microscopy, taking Ho_2O_3–Y_2O_3 mixed oxides as an example. Because the emission from an RE ion is sensitive to its local environment, care has to be taken not to confuse effects of variations in chemical composition with stress-induced effects caused by imperfections within the crystallites. This is demonstrated in Fig. 5 for the sample containing 20 mol% Ho. In the upper map, the intensity ratio defined above is plotted in a gray scale map, with light gray tones corresponding to lower values of $I(528)/I(540)$ and dark gray tones corresponding to higher values. This map was produced for a sample calcined at 1173 K. The lower map is drawn to the same scale, and contains data obtained for the sample annealed at 1570 K. Two things are noteworthy: after annealing, the ratio $I(528)/I(540)$ is higher, and local variations diminish. On the basis of the 300 values available for each sample, the mean value and the standard deviation calculated for the parameter $I(528)/I(540)$ are 0.23 ± 0.03 in the case of the calcined sample (1173 K) and 0.29 ± 0.01 in the case of the annealed sample (1570 K). Tentatively, we suggest that the latter value of the standard deviation gives a measure of the variation in chemical composition of the sample investigated. Such an interpretation relies on the assumption that the distance of diffusion of the cations in the crystallites is smaller than the spatial resolution of the mapping experiment at the temperature employed. That the intensity ratio increases after annealing

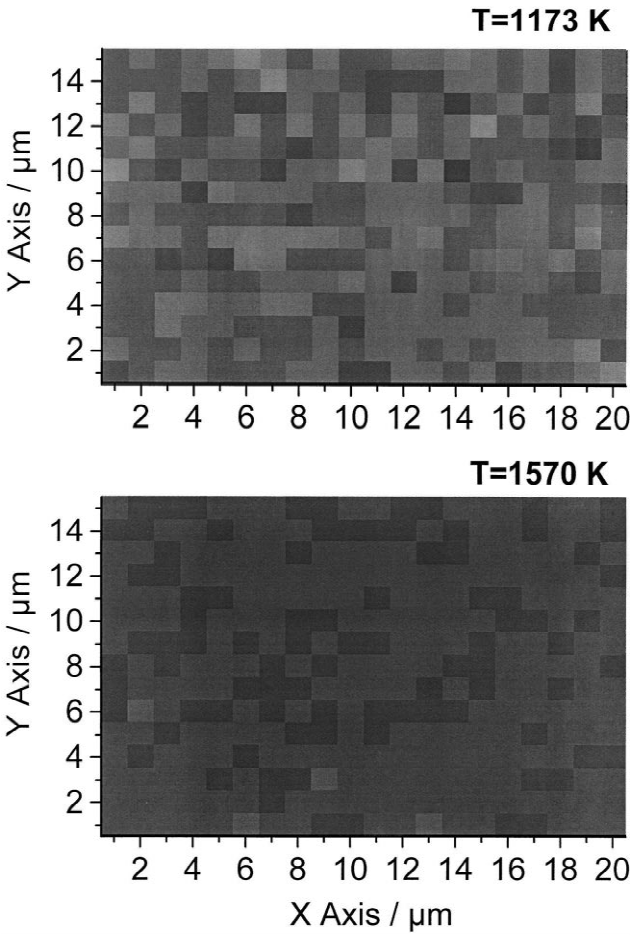

Fig. 5. Maps of the intensity ratio $I(528)/I(540)$ obtained for the sample with 20 mol% Ho. Lower map: sample annealed at 1570 K; upper map: sample calcined at 1173 K. Both maps are drawn to the same scale. Light gray tones equal low values, and dark gray tones equal high values of $I(528)/I(540)$.

indicates that the thermal history of the sample is important. Further investigations will be performed to clarify this point.

In summary, we have demonstrated that Raman and emission spectroscopy provide alternatives to established analytical methods, especially when coupled with confocal microscopy in order to achieve spatially resolved characterization.

Acknowledgements

The support of the Research Foundation of the Swiss Gas Industry (FOGA) is gratefully acknowledged. We are grateful to Loris Scandella, who recorded the SEM micrographs.

References

[1] C.K. Jørgensen, H. Bill, R. Reisfeld, J. Lumin. 24/25 (1) (1981) 91.
[2] J. Werth, in: Proceedings of the 17th Power Sources Conference, 1963, p. 23.
[3] T.J. Coutts, C.S. Allman, J.P. Benner (Eds.), Thermophotovoltaic Generation of Electricity. Third NREL Conference on Thermophotovoltaics, AIP Conference Proceedings, Vol. 401, American Institute of Physics, 1997.
[4] J.-C. Panitz, J.-C. Mayor, A. Brunner, W. Durisch, M. Schubnell, Development of thermophotovoltaic energy converters, PSI Annual Report 1997, Annex V, Paul Scherrer Institut, 1998, p. 33.
[5] J.-C. Panitz, M. Schubnell, W. Durisch, F. Geiger, in: T.J. Coutts, C.S. Allman, J.P. Benner (Eds.), Third NREL Conference on Thermophotovoltaics, Thermophotovoltaic Generation of Electricity, AIP Conference Proceedings, Vol. 401, American Institute of Physics, 1997, p. 265.
[6] J.-C. Panitz, J. Raman Spectrosc. 30 (1999) 1035.
[7] L.A. Chick, L.R. Pedersen, G.D. Maupin, J.L. Bates, L.E. Thomas, G.J. Exarhos, Mater. Lett. 10 (1990) 6.
[8] J.-C. Panitz, Appl. Spectrosc. 51 (1997) 1073.
[9] G. Schaak, J.A. Koningstein, J. Opt. Soc. Am. 60 (1970) 1110.
[10] J. Gouteron, J. Zarembowitch, A.M. Lejus, C.R. Acad. Sci. Paris 289 (1979) C243.
[11] J.B. Gruber, R.D. Chirico, E.F. Westrum Jr., J. Chem. Phys. 76 (1982) 4600.
[12] L.A. Tucker, F.J. Carney Jr., P. McMillan, S.H. Lin, L. Eyring, Appl. Spectrosc. 38 (1984) 857.
[13] M.W. Urban, B.C. Cornilsen, J. Phys. Chem. Solids 48 (1987) 475.
[14] Y. Repelin, C. Proust, E. Husson, J.M. Beny, J. Solid State Chem. 118 (1995) 163.
[15] A.S. Barker, A.J. Sievers, Rev. Mod. Phys. 47 (Suppl. 2) (1975) S1.
[16] H. Ishibashi, K. Shimomoto, K. Nakahigashi, J. Phys. Chem. Solids 55 (1994) 809.